Modulation of formin processivity by profilin and mechanical tension

Mikael Kerleau[1†], Luyan Cao[1†], Emiko Suzuki[1], Hugo Wioland[1], Sandy Jouet[1], Bérengère Guichard[1], Martin Lenz[2], Guillaume Romet-Lemonne[1*] & Antoine Jégou[1*]

[1] Institut Jacques Monod, CNRS, Université Paris Diderot, Paris, France.
[2] LPTMS, CNRS, Université Paris-Sud, Université Paris-Saclay, 91405 Orsay, France.
[†] contributed equally to this work
* corresponding authors

ABSTRACT

Formins are major regulators of actin networks. They enhance actin filament dynamics by remaining processively bound to filament barbed ends. How biochemical and mechanical factors affect formin processivity are open questions. Monitoring individual actin filaments in a microfluidic flow, we report that formin mDia1 dissociates faster under higher ionic strength and when actin concentration is increased. Profilin, known to increase the elongation rate of formin-associated filaments, surprisingly decreases the formin dissociation rate, by bringing formin FH1 domains in transient contact with the barbed end. In contrast, piconewton tensile forces applied to actin filaments accelerate formin dissociation by orders of magnitude, largely overcoming profilin-mediated stabilization. We developed a model of formin conformations and its confrontation to our data indicates the existence of two different dissociation pathways, with force favoring one over the other. How cells limit formin dissociation under tension is now a key question for future studies.

INTRODUCTION

The diversity of actin filament networks in cells stems from a few key nucleators, such as formins and the Arp2/3 complex, which have very specific activities (Blanchoin et al., 2014; Bovellan et al., 2014; Wales et al., 2016). In cells, formins are responsible for the generation of elongated, unbranched actin filament structures such as the ones found in filopodia, stress fibers, the cytokinetic ring, and within the nucleus (Isogai and Innocenti, 2016). Formin malfunction is linked to a number of pathologies, such as angiogenesis (Phng et al., 2015), neuropathies (Roos et al., 2015) and cancer (Choi et al., 2015).

Formins function as homodimers and most isoforms share a similar mode of activation, where the interaction of activators with N-terminal domains releases auto-inhibition and mediates the anchoring of formins to membranes. Formin functional domains, Formin Homology Domains 1 (FH1) and 2 (FH2), are responsible for their most salient features: their ability to track both growing and depolymerizing filament barbed ends and to accelerate their elongation from profilin-actin (Higashida et al., 2004; Jégou et al., 2013; Kovar and Pollard, 2004; Mizuno et al., 2011; Romero et al., 2004). Rapid elongation is achieved by the FH1 domains, seen as flexible chains containing polyproline tracks, which bind profilin-actin complexes and deliver them to the barbed end (Higashida et al., 2004; Kovar and Pollard, 2004; Romero et al., 2004). Barbed end tracking is achieved by the translocation of the FH2 dimer, which encircles the actin subunits at the barbed end (Otomo et al., 2005).

Formin processivity, quantified by the dissociation rate of the formin from the barbed end, determines for how long filaments interact with a formin. While a formin resides at the barbed end, it decreases its affinity for Capping Protein (Bombardier et al., 2015; Shekhar et al., 2015), modulates its elongation, and can maintain it anchored to a membrane. Processivity is thus a pivotal characteristic, determining formins' ability to shape filament networks and transmit forces. Formin processivity has long been identified as an essential feature of formins and occasional measurements have revealed quantitative differences between isoforms (Bilancia et al., 2014; Kovar et al., 2006; Paul and Pollard, 2008; Romero et al., 2004; Vizcarra et al., 2014). Negative regulators bind to FH2 to displace formin from filament barbed end (Chesarone et al., 2009; Chesarone-Cataldo et al., 2011), whereas Ena/VASP, via its EVH1 domain, is able to bind to FH1 domains without impacting formin processivity (Bilancia et al., 2014). While processivity seems mainly governed by FH2-actin interactions, the DAD domain (or "tail"), found next to the FH2 domain at the C-terminus, has been reported to contribute to the processivity of Drosophila formin Capuccino (Vizcarra et al., 2014). The dissociation rate of yeast formin Bni1p has been proposed to scale with filament elongation velocity, suggesting the existence of a transient, weakly bound state occurring upon actin subunit addition (Paul and Pollard, 2008).

Today, many important aspects of formin processivity remain unclear. The possible involvement of formin's other domains and the modulation of formin processivity by various physiological factors have yet to be determined. In particular, pulling forces such as the ones exerted on actin filaments in cells (Romet-Lemonne and Jégou, 2013) have been reported to modulate formin elongation (Courtemanche et al., 2013; Jégou et al., 2013; Kubota et al., 2017; Yu et al., 2017; Zimmermann et al., 2017) but their impact on processivity is an open question.

Here, we systematically quantify the dissociation rate of mammalian formin mDia1 in different *in vitro* conditions. Using microfluidics to monitor and manipulate individual actin filaments (Figure 1), we find that the dissociation rate is modulated by ionic strength (Figure 2) as well as by actin and profilin concentrations (Figure 3). Profilin prolongs formin residence at the barbed end via its interaction with the FH1 domain, allowing rapid elongations without enhancing formin dissociation. We find that tension applied on filaments has a dramatic impact on formin dissociation rate, which increases by several orders of magnitude, independently of other parameters (Figure 4). A mathematical model describing the possible formin states at the barbed end is developed and confronted to our experimental data (Figure 5). It indicates that, when an actin subunit is added to the barbed end, formin mDia1 goes through a dissociation-prone transition, which is relatively insensitive to force, and which can be stabilized by FH1-profilin-barbed end interactions.

RESULTS

Single-filament microfluidics is an efficient means to measure formin processivity under various conditions

We have carried out experiments using a standard microfluidics chamber with three inlets, in different configurations (Figure 1A-C and Methods). Using anchored spectrin-actin seeds we have monitored the growth of free actin filaments barbed ends, which we exposed to a solution of formin for typically ten seconds and resumed exposing to constant concentrations of actin and profilin. The presence of formin at the barbed end was visible thanks to its faster elongation (in the presence of profilin). This configuration was used with fluorescently labeled actin (Figure 1A) or alternating exposure to labeled actin with unlabeled actin, producing striped filaments, which allowed us to measure formin related rate constants when incorporating fully unlabeled actin segments (Figure 1B, Methods). Another configuration consisted in anchoring formins to the coverslip surface, nucleating and elongating filaments from these formins (Figure 1C). This allowed us to monitor the elongation of filaments from unlabeled actin, and the dissociation of the formin from the barbed end was revealed by the detachment of the filament which is then carried away by the flow. This configuration applies calibrated forces to the filament-formin interaction (Jégou et al., 2013), which can be kept very low (< 0.1 pN) using a low microfluidics flow rate, or made significant, up to several pN, by increasing the flow rate (Figure 4). Except for the variant with striped filaments, we have used these experimental configurations in earlier studies (Jégou et al., 2013; Montaville et al., 2014; Shekhar et al., 2015).

These different configurations allowed us to measure, under a given set of conditions, the survival fraction of filaments that still bear a formin at their barbed end as a function of time (Figure 1E), giving access to the formin dissociation rate constant k_{off}. The experimental configurations shown in Figure 1B and 1C were specifically used to determine k_{off} with unlabeled actin or with no profilin. We have verified that the results were not affected by our choice of experimental configuration.

We used purified actin from rabbit muscle, either unlabeled or labeled on lysine 328 with Alexa 488 (Tóth et al., 2016). We used recombinant formin constructs (figure 1D): mDia1(FH1-FH2-DAD) with full length functional domains; a truncated mDia1(FH1(2PP)-FH2-DAD) construct with an FH1 domain that contained only the two polyproline (PP) tracks closest to the FH2 domain; and mDia1(FH2-DAD) which contained no FH1 domain at all. Unless specified otherwise, “formin” refers to mDia1(FH1-FH2-DAD).

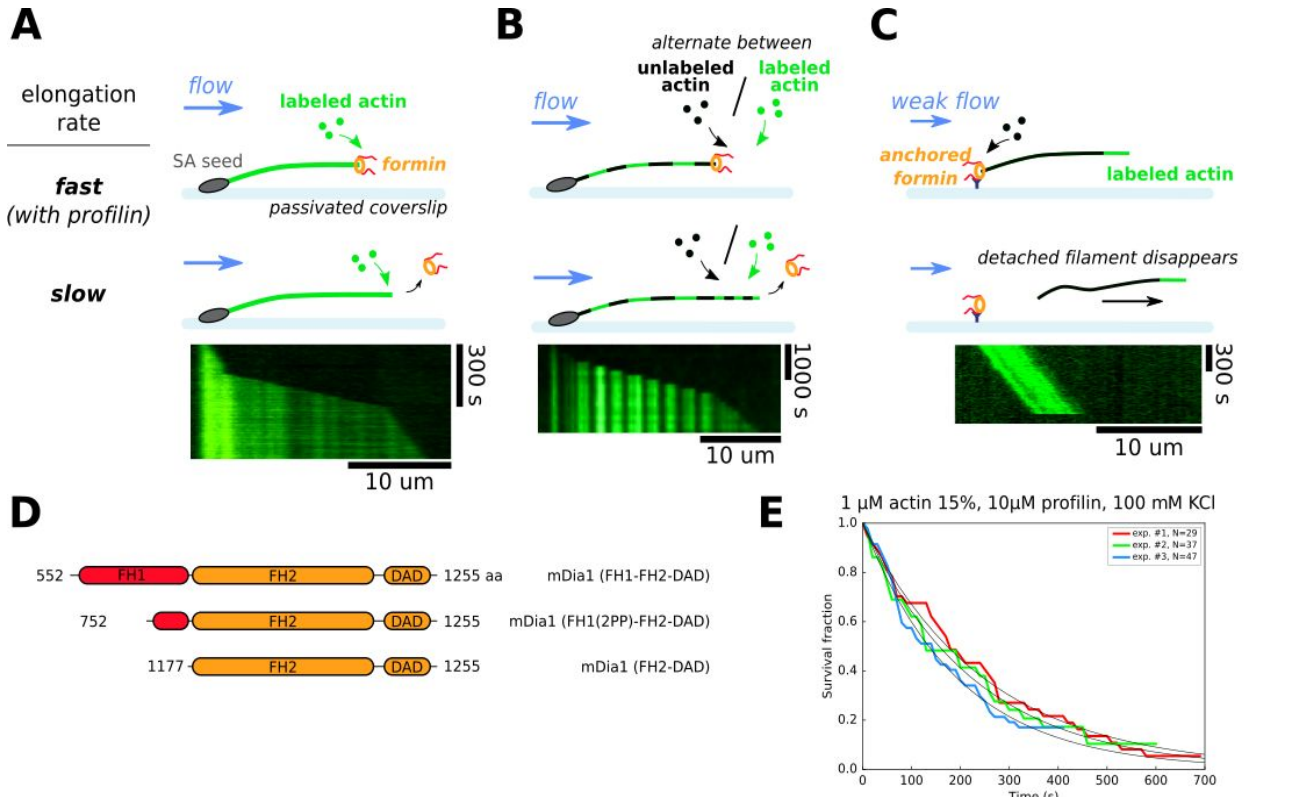

Figure 1. Single-filament microfluidics experimental configurations to measure formin processivity
A-C. Different experimental configurations using microfluidics for the study of formin processivity, showing sketches of the side view (top) and typical kymographs of individual filaments (bottom).
A. Alexa 488 labeled actin filaments are elongated from surface-anchored spectrin-actin seeds. Transient exposure to a formin solution puts formins on filament barbed ends, which elongate faster (here in the presence of 1µM 15% Alexa 488 labeled actin + 5 µM profilin, at 100 mM KCl). Upon formin dissociation, the barbed end elongates slower. Images were acquired in TIRF microscopy. See Supp. Movie S1.
B. Same configuration as in (A), but the filaments are exposed to a periodic alternation of different conditions: here a solution of unlabeled actin (0.3 µM actin, 50 mM KCl) for 100 seconds and a solution of 15% Alexa 488 labeled actin (0.5 µM actin + 2 µM profilin, 50 mM KCl) for 20 seconds. Images were acquired in epifluorescence while exposing to unlabeled actin. See Supp. Movie S2.
C. Configuration where formins are anchored to the surface by their C-terminus. Filaments were nucleated using a solution of labeled actin, and elongated by flowing in a solution of unlabeled actin (here, 0.3 µM actin, at 50 mM KCl), until the filaments eventually detached and disappeared. The viscous drag applied on the filaments was kept low (<0.1 pN) by working with low flow rates. Images were acquired in epifluorescence. See Supp. Movie S3.
D. Domain architecture and boundaries for the mDia1 constructs used in this study.
E. Survival fractions of formin-bound barbed ends as a function of time, obtained from three independent experiments performed in the same conditions, in the experimental configuration shown in (A). Curves are fitted by a mono-exponential decay to obtain formin dissociation rate k_{off}.

Impact of ionic strength and actin labeling on formin processivity

Varying KCl concentration in our assay buffer (see Methods), we found that the ionic strength had a strong impact on formin dissociation (Figure 2A,B). In comparison, the same variations of the ionic strength had a limited impact on the barbed end elongation rate, with or without formins

(Figure 2B, inset). In order for formin dissociation rates to be in a range that could be measured accurately, we have used either 100 mM KCl (for experiments with no mechanical tension, Figure 2 and 3) or 50 mM KCl (for experiments with pulling forces, Figure 4). We have verified that the effects we report in the rest of this paper are not qualitatively affected by the choice of ionic strength (Supp. Fig. S1).

Labeling actin with a fluorophore can hinder its polymerization or its interaction with regulatory proteins (Chen et al., 2012; Kuhn and Pollard, 2005) and lead to unsuspected artefacts (Niedermayer et al., 2012). Here, our labeling of actin on lysine 328 with Alexa 488 fluorophore had no measurable impact on the elongation rate of formin-free barbed ends, but slowed down their elongation with formins significantly and enhanced formin dissociation rate (Figure 2C,D). Using our microfluidics setup to measure reaction rates with unlabeled actin (Figure 1B,C), we have verified that the conclusions we drew from the observation of 15% Alexa488-labeled actin filaments were not biased by labeling (Supp. Fig. S1).

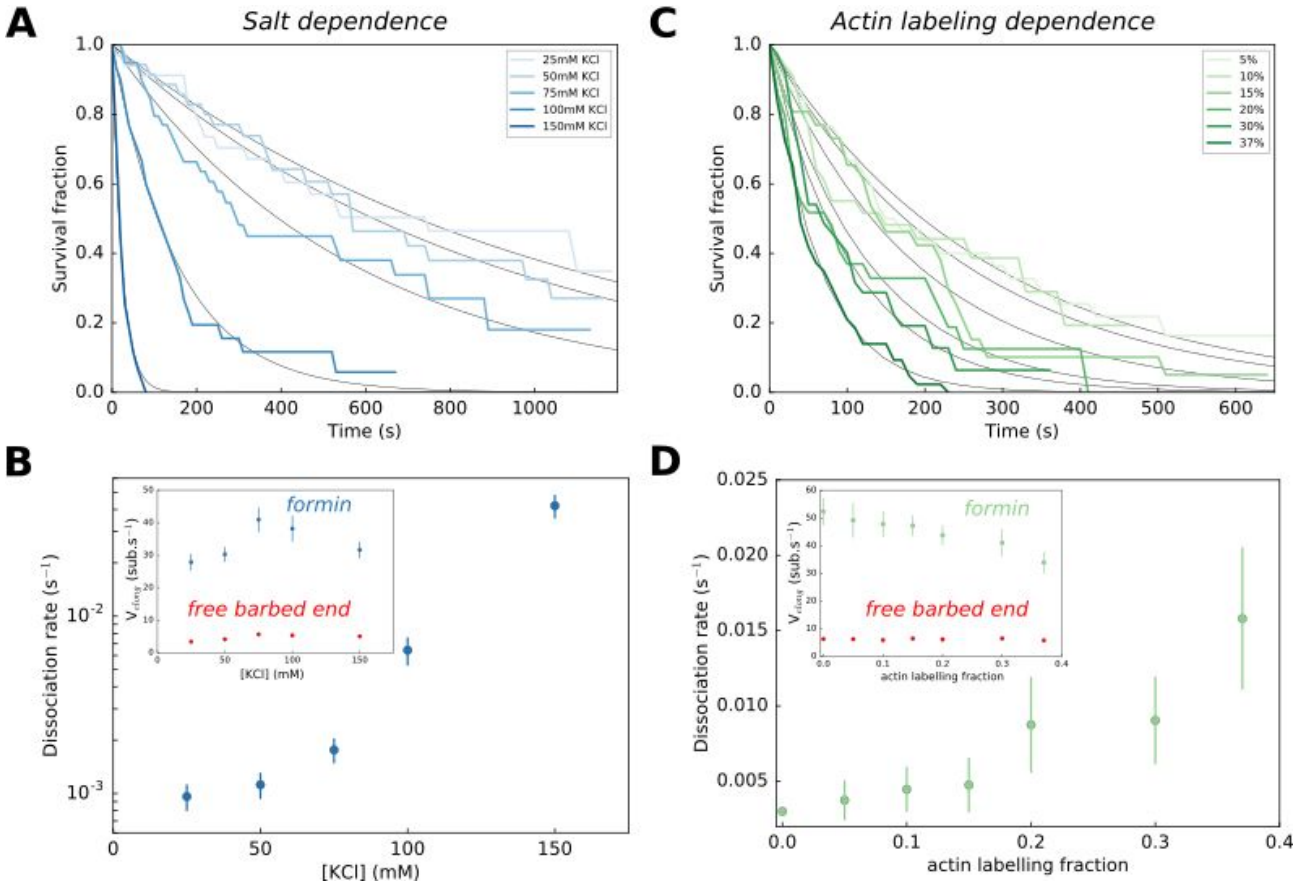

Figure 2. Impact of salt and actin labeling fraction of formin processivity

A,B. Effect of salt concentration on the survival fraction of formin-bound barbed ends (A), on the formin dissociation rates (B, log-linear scale) as well as on the barbed end elongation rates (B, inset). The dissociation rates in (B) result from the exponential fits (black lines) shown in (A). Each data point corresponds to a population of 30-40 filaments.

C,D. Effect of the actin Alexa 488 labeling fraction on the survival fraction of formin-bound barbed ends (C), on the formin dissociation rates (D) and on the barbed end elongation rates (D, inset). Each data point in (D) corresponds to a population of 30-40 filaments.

Error bars on formin dissociation rates indicate 65% confidence intervals based on exponential fits and sample size (see Methods), and error bars on elongation rates indicate standard deviations.

Profilin increases formin processivity, involving FH1 domains

For a given profilin concentration, the barbed end elongation rate v_{elong} scales with the actin concentration (with or without formin, Supp. Figure S2) and we observed that the formin dissociation rate k_{off} increased with actin concentration, and thus with the elongation rate (Figure 3A). This confirmed earlier observations on yeast formin Bni1p (Paul and Pollard, 2008). However, the amplitude of the increase of the formin dissociation rate with actin concentration appeared to depend significantly on profilin concentration. As a result, there is no universal scaling of k_{off} with the elongation rate. In fact, using different sets of actin and profilin concentrations, one can obtain identical elongation rates with very different formin dissociation rates (Figure 3A).

To investigate this point further, we measured the formin dissociation rate as a function of profilin concentration at a fixed actin concentration and found that k_{off} decreased with increasing profilin concentration (Figure 3B). In contrast with actin, the modulation of the elongation rate by profilin is biphasic (Kovar et al., 2006): low profilin concentrations increase v_{elong} as actin becomes profilin-actin, while higher concentrations slow down elongation as excess profilin competes with profilin-actin for polyproline binding sites on FH1 domains and barbed ends (Figure 3B inset). Importantly, the decrease of k_{off} was also observed in the lower range of profilin concentrations, where the elongation rate greatly increases with profilin. It thus appears that profilin itself reduces formin detachment, independently of the barbed end elongation rate.

In order to estimate the role of the FH1 domains in the profilin-induced reduction of the dissociation rate, we repeated these measurements using a truncated formin construct, where both FH1 domains of the formin homodimer only contained 2 profilin-binding polyproline tracks. We found that the truncated formin still enhanced filament elongation from profilin-actin, though not as strongly as the formin with full-length FH1 (Figure 3B inset). It still exhibited a reduction of k_{off} with profilin concentration (Figure 3B), but the dissociation rate of FH1(2PP)-FH2-DAD was consistently higher than of wild type FH1-FH2-DAD for all profilin concentrations tested. These results confirm that the formin dissociation rate does not generally scale with the elongation rate,. They also suggest that FH1 polyproline tracks, which are responsible for rapid elongation, are also responsible for the decrease of k_{off} in the presence of profilin.

To further investigate the contribution of the FH1 domains, we then asked whether the reduction of the dissociation rate by profilin required its binding to the FH1 domain, or if the rapid equilibrium of profilin with the barbed end was enough to stabilize its interaction with the formin. We reasoned that if the latter hypothesis was correct, the processivity of mDia1(FH2-DAD) dimers (with no FH1 domains) should be enhanced by the binding of profilin to the barbed end. To test this, we compared the FH2 dimer dissociation rate for different barbed end elongation rates, obtained in the presence or absence of profilin (Figure 3D). We found that the presence of a large excess of profilin, which significantly puts the barbed end in a profilin-bound state and slows down its elongation (Jégou et al., 2011; Pernier et al., 2016), led to the same FH2 dimer dissociation rate as when the same elongation rates were reached without profilin. These results indicate that FH1 is required in order for profilin to decrease the formin dissociation rate k_{off}. In the absence of profilin, FH1-FH2 behaved like FH2 (Figure 3D), indicating that the presence of FH1 domains alone, in the absence of profilin, has no impact on processivity.

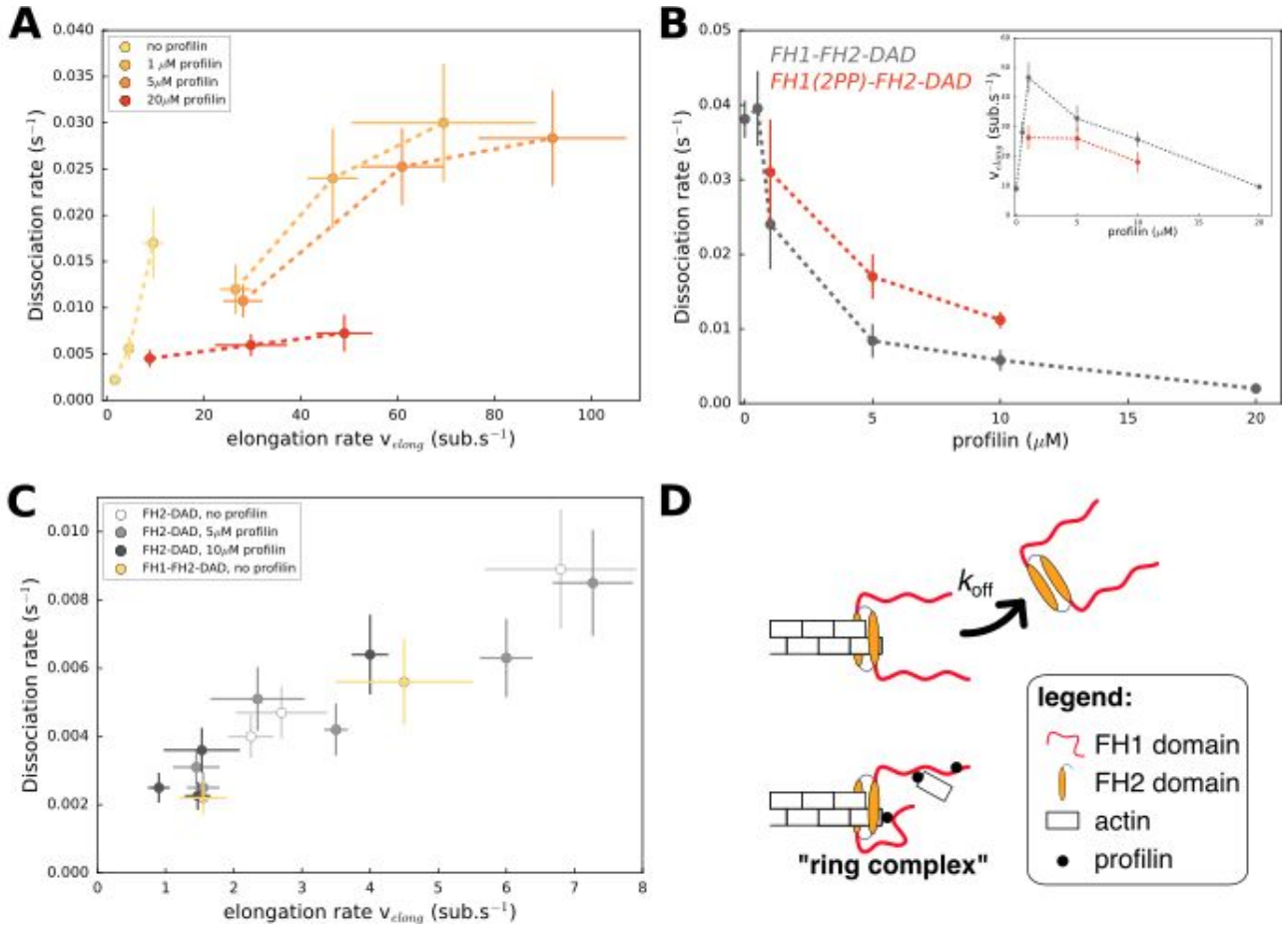

Figure 3. Formin dissociation is enhanced by G-actin concentration, and slowed down by profilin.
A. Variation of the formin dissociation rate as a function of the barbed end elongation rate. Each data set (N=30-40 filaments) was obtained with a fixed profilin concentration and different actin concentrations, at 100mM KCl. Each point corresponds to an independent experiment, performed with 15% Alexa488-labeled actin, except for the data without profilin which were acquired with unlabeled actin.
B. Variation of the formin dissociation rate and the barbed end elongation rate (inset) as a function of profilin concentration, for formins with a full length FH1 (FH1-FH2-DAD) and with a truncated FH1 containing only two polyproline tracks (FH1(2PP)-FH2-DAD). The data was obtained with 15% Alexa 488-labeled actin, at 100 mM KCl. The same profilin dependence was observed using unlabeled actin, for both 50 and 100 mM KCl (Supp. Figure S1). Each data point corresponds to the average of 1-3 independent experiments.
C. Variation of the formin dissociation rate as a function of the barbed end elongation rate: for FH2-DAD homodimers in the presence or absence of profilin, and for FH1-FH2-DAD in the absence of profilin, all with unlabeled actin.
D. Sketch illustrating the profilin-mediated interaction between FH1 and the barbed end, forming the “ring complex”, which appears to prevent the dissociation of formin from the barbed end.
Error bars on formin dissociation rates indicate 65% confidence intervals based on exponential fits and sample size (see Methods), and error bars on elongation rates indicate standard deviations.

Mechanical tension strongly decreases formin processivity

In cells, anchored formins are exposed to mechanical tension applied to actin filaments, typically as a consequence of myosin activity. We thus investigated the impact of such forces on formin

processivity. To do so, we performed experiments with surface-anchored formins, in the configuration shown in Figure 1C, but using higher flow rates in order to apply significant tension to the filaments (Figure 4A). In a previous study, we have shown that the force at the anchoring point scales with the filament length (Jégou et al., 2013), and thus increases as the filaments elongate over time. Here, the sigmoidal shape of the survival fractions over time indicated an increase of the dissociation rate k_{off} with the applied force (Figure 4B). In order to avoid making assumptions regarding the force-dependence of the dissociation rate k_{off}, we determined k_{off} at different forces by local fits of the survival fractions (see Methods). We verified that the filament detachment events observed during the experiment corresponded to filament-formin dissociations (as sketched in Figure 4A) by checking that formins were still on the surface at the end of the experiment (see Methods and Supp Figure S4).

We found that mechanical tension had a dramatic impact on the formin dissociation rate, which increased by a few orders of magnitude when piconewton forces were applied (Figure 4C-E). Interestingly, the differences in dissociation rate linked to differences in actin concentrations seemed to disappear when force is applied : the weaker values of k_{off} increased more steeply with force, resulting in a convergence of the dissociation rates when tension was applied (clearly visible in the log-linear representation of Figure 4C and Supp Figure S3A). Likewise, the dissociation constant increased with tension in a seemingly identical fashion whether the filaments were elongating from actin alone or with an excess of profilin (Figure 4D and Supp Figure S3B).

We found a similar increase of k_{off} with tension for FH2 dimers (i.e. without FH1 domains, Figure 4E), and for FH1-FH2 dimers anchored via their FH1 or their FH2 domains (i.e. whether force is applied to FH2 alone or to FH1 as well, Figure 4F). These observations indicate that FH1 domains do not participate in the mechanical modulation of formin processivity.

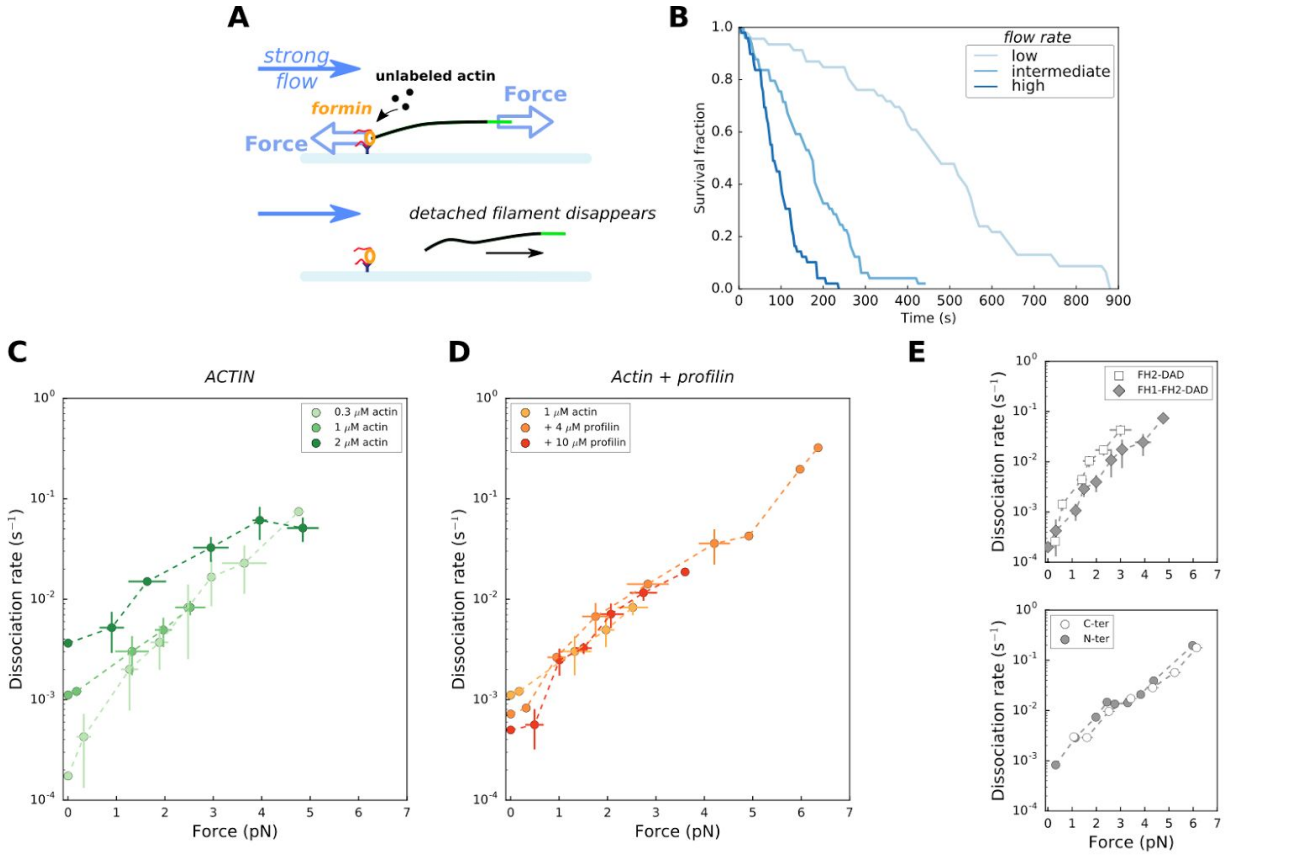

Figure 4. Force has a great impact on formin processivity.
A. Sketch of the experimental configuration, similar to that of Figure 1C, but where significant forces are applied using various flow rates. The applied force scales with the filament length. Experiments were carried out by elongating the filaments with unlabeled actin, at 50 mM KCl.
B. Survival fractions of surface-anchored filaments, elongating with 1µM actin + 10µM profilin, using different flow rates to reach different force ranges: each filament underwent 0.051 pN/µm (blue points, N=46 filaments), 0.204 pN/µm (green, N=49) or 0.501 pN/µm (purple, N=49); and the average initial filament length was 4.9 µm (blue), 3.2 µm (green) and 2.6 µm (purple).
C-E. Formin dissociation rate as a function of applied force (log-linear plots), for different actin concentrations in the absence of profilin (C); for 1 µM actin with different profilin concentrations (D); for 0.3µM actin in presence or absence of FH1 domains (E, top); and for 1 µM actin, 4µM profilin for FH1-FH2-DAD formins either anchored by their FH1 N-terminus or FH2 C-terminus (E, bottom). Dissociation rates were obtained by local fits of the slope in survival fractions similar to the ones shown in (B) (see Methods). Each data point is either obtained from a single experiment or is the average of 2-3 independent experiments. The data points at zero force were measured independently, using the configuration shown in figure 1B (striped filaments). The error bars indicate standard deviations when several independent experiments were grouped (data from individual experiments for (C) and (D) are shown in Supp. Fig. S3).

DISCUSSION

Processivity mostly relies on FH2-filament interactions, with an unexpected contribution of FH1 domains

Formin control of actin filament elongation at the barbed end is mediated by its homology domains FH1 and FH2, as well as its tail domain, DAD (Gould et al., 2011; Vizcarra et al., 2014). We quantified formin processivity by measuring its dissociation rate k_{off}. Our data indicate that FH2-barbed end interactions are destabilized by ions (Figure 2A). These results confirm that salt bridges mediating FH2-actin interactions, which have been predicted from molecular dynamics simulations (Baker et al., 2015), are essential determinants of the residence time of formin at the barbed end. Our data also indicate that FH2-actin interactions are destabilized by the presence of a fluorescent label on actin subunits (Figure 2C), consistent with the notion that the lateral contacts of FH2 with actin subunits are essential to maintain the formin at the barbed end (Otomo et al., 2005).
Unexpectedly, we show here that FH1 domains also contribute to keeping formin at the barbed end (Figure 3). These results appear in good agreement with the proposition that FH1 delivers profilin-actin to the barbed end by forming a “ring complex” (Vavylonis et al., 2006), where profilin simultaneously interacts with the barbed end and one polyproline track of one of the two FH1 domains. The ring complex is also likely formed when profilin is brought to the barbed end by FH1 without an actin monomer. It seems natural that, in such a configuration, the FH1 domains would constitute an obstacle to the dissociation of the FH2 dimer from the filament barbed end (Figure 3D).

This contribution of FH1 domains also confers a new function to profilin: not only does it allow a rapid barbed end elongation, it also helps maintain formin at the barbed end. If rapid elongation were to be achieved without profilin, formins would dissociate very rapidly (Figure 3A).
We have also shown that, when FH1 domains were severely truncated, reducing their number of polyproline tracks from 14 to 2, they were still able to perform their tasks regarding both the acceleration of elongation and the reduction of dissociation in the presence of profilin (Figure 3B).

These observations are consistent with earlier results on yeast formin Bni1p showing that polyproline tracks located closer to the FH2 domain were the main contributors to FH1 activity (Courtemanche and Pollard, 2012).

This FH1-profilin-mediated stabilization does not seem to resist pulling forces, since the formin dissociation rate increases equally fast in the presence of profilin as without profilin (Figures 4C,D), or even when FH1 domains are absent (Figure 4E).

Modeling FH2 conformations at the barbed end

Putting the contributions of FH1 domains and profilin aside, our results show that the elongation velocity, hence the addition of actin subunits, enhances formin dissociation from the barbed end (Figure 3A). This suggests that the FH2 dimer goes through a transient, weakly bound state, every time a new actin subunit is added (Figure 5A), as already proposed by (Paul and Pollard, 2008). Based on this idea, we have built a mathematical model predicting the elongation velocity v_{elong} and dissociation rate k_{off} for a barbed-end associated formin as a function protein concentrations and force. This model and its predictions are presented in detail in the Supplementary Text.

As our model includes a substantial number of chemical reactions and associated reaction rates, we focus less on obtaining precise fits to the experimental data - which are somewhat trivial and uninformative when a large number of adjustable parameters are involved - and instead demonstrate that the *qualitative* shape of the curves predicted by our model is consistent with our experimental measurements. This shows that the agreement between our model and the data is essential, and not an accident of a specific set of values for the fitting parameters.

Our model, while it does not attempt to explicitly describe the details of FH1 activity, as done by Vavylonis and colleagues (Vavylonis et al., 2006), does include an effective affinity of profilin for barbed ends, and is able to account for our experimental data on profilin by simply considering that the presence of profilin at the barbed end blocks formin dissociation (Supplementary Text and figures therein). Our model thus ties together our observations in a global, consistent description. It also provides insights into the FH2 dimer conformations and the effect of applied tension, which we now summarize here.

Structural details of Bni1p(FH2)-actin interactions (Otomo et al., 2005) have led to the proposal that, as they wait for the addition of a new actin subunit, the FH2 dimer and the barbed end are in a rapid equilibrium between an elongation-competent “open” state and an elongation-forbidding “closed” state. In the frame of the subsequently proposed “stair-stepping” model, FH2 hemidimer translocation (along the filament’s main axis and over a distance of one actin monomer size) is associated to this rapid equilibrium. In contrast, the “stepping-second” model proposes that the open-closed equilibrium involves no such FH2 hemidimer translocation, which would instead take place after each subunit addition and thus be related to the aforementioned transition state (Paul and Pollard, 2008).

Our earlier work showing that tension accelerates mDia1-mediated elongation (Jégou et al., 2013)ore recent work applying tension with magnetic tweezers (Yu et al., 2017), both indicate that the open-closed equilibrium corresponds to a working distance of one monomer size, consistent with the stair-stepping model. We have thus chosen this model for our schematic representations

of the open-closed equilibrium (Figure 5), even though our data on formin dissociation does not favor one model over the other. The conclusions we draw from our present model of formin dissociation do not require the stair-stepping context.

Our model for dissociation primarily includes the notion that the FH2 dimer goes through a transient, dissociation-prone conformation every time a new actin subunit is added. As sketched in Figure 5A, formin can thus dissociate following two routes: (1) the FH2 dimer unbinds from the barbed end from the open state during its rapid open-closed equilibrium, with a rate $k_{off}^{O}(f)$, or (2) the FH2 dimer unbinds during the transition state that follows subunit addition, with a rate $k_{off}^{T}(f)$. In the absence of force, our data show a strong dependence of formin dissociation on actin concentration, i.e. on elongation rate (Figure 3A) meaning that $k_{off}^{T}(f=0)$ is the dominant contribution to the global $k_{off}(f=0)$. When pulling forces are applied, the formin dissociation rates for different actin concentrations converge, *i.e.* $k_{off}(f)$ does not depend on actin concentration anymore (Figure 4C). The model predicts such a behavior when $k_{off}^{O}(f)$ increases with force more strongly than $k_{off}^{T}(f)$, and thus becomes dominant at high forces (Figure 5B). In contrast, the situation where $k_{off}^{T}(f)$ remains the dominant contribution to dissociation results in curves for $k_{off}(f)$ at different actin concentrations that remain well separated at high forces (Figure 5C). The confrontation of our model to our experimental data thus indicates that, while dissociation from the transition state is the dominant route at low force, it is the dissociation from the open state that dominates at high force.

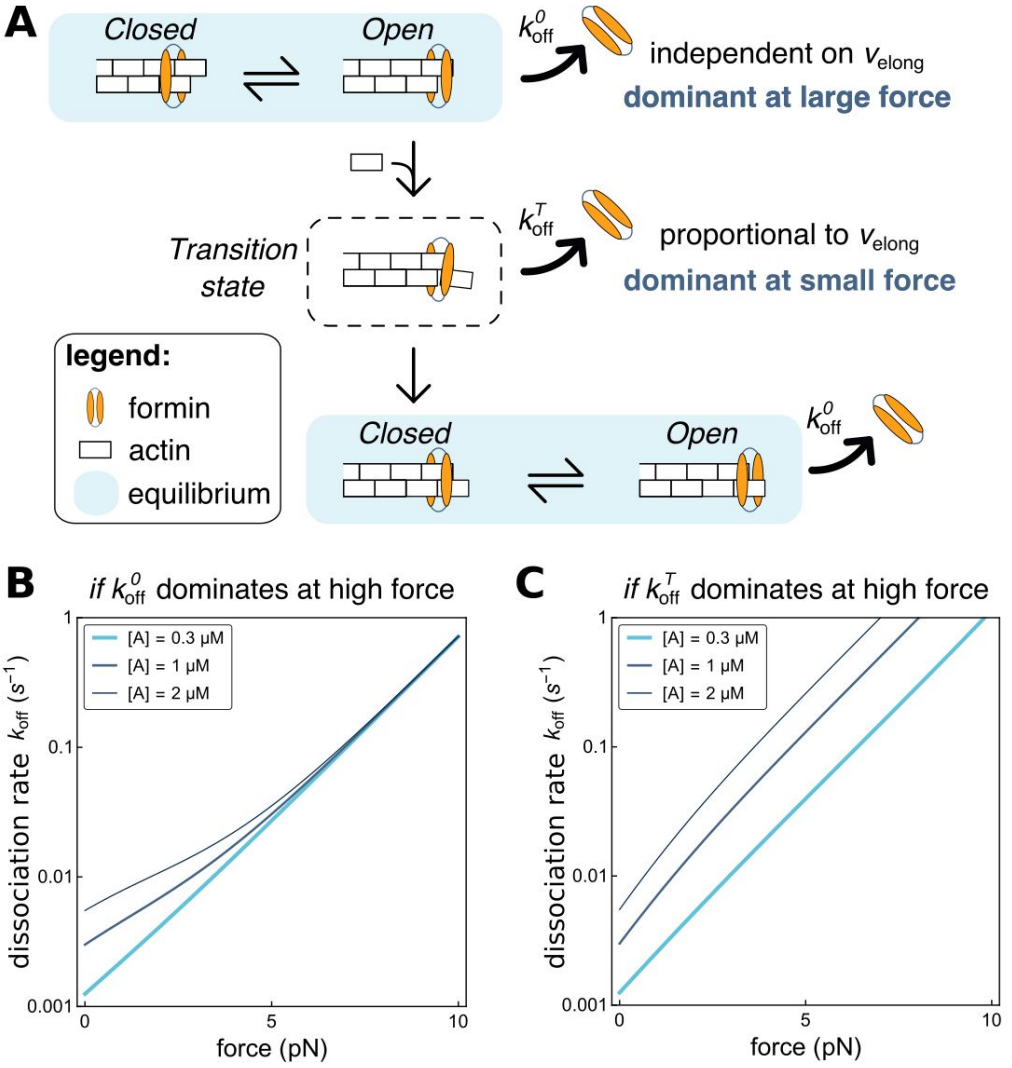

Figure 5. Modeling formin dissociation, in the absence of profilin.
A. Sketch summarizing the conformations adopted by the FH2 dimer and the actin filament barbed end in our model, in the absence of profilin (for a complete description of the model, see Supplementary Text). The system is in rapid equilibrium between an open and a closed state (depicted here as in the "stair-stepping" model) and only the open state allows the addition of a new actin subunit at the barbed end. Following this elongation event, the system is in a Transition state, which decays rapidly into a new open-closed rapid equilibrium. Formin dissociation from the barbed end can occur while the system is in the open state (with rate k_{off}^{O}) or in the transition state (rate k_{off}^{T}). The global, observable dissociation rate k_{off} comprises these two routes.
B,C. Predictions of the model for the variation of the dissociation rate k_{off} as a function of force, in log-linear representations. In both cases, k_{off}^{T} is the dominant contribution at zero force. In B, k_{off}^{O} increases more strongly than k_{off}^{T} when force is applied and thus becomes dominant at high force (computed with working distances $\boldsymbol{\delta}_O=\boldsymbol{\delta}$ and $\boldsymbol{\delta}_T=0$, see Supplemental Text). In C, k_{off}^{T} increases more strongly than k_{off}^{O} when force is applied ($\boldsymbol{\delta}_O=0$ and $\boldsymbol{\delta}_T=\boldsymbol{\delta}$, see Supplemental Text).

How do cells manage formin dissociation in a mechanical context?

Our results show that mechanical tension plays a dominant role in the modulation of formin processivity. The dramatic enhancement of formin dissociation, upon application of piconewton

forces, appears difficult to compensate with the other factors we have tested, such as actin and profilin concentrations. In cells, where filaments are likely to be tensed mainly because of myosin activity, our results raise questions regarding how these filaments may remain in interaction with membrane-anchored formins. Since it seems unlikely that filaments detach from membranes as soon as moderate forces are applied, they may cumulate alternative anchoring strategies, or see their interaction with formins reinforced by other factors.

In cells, formin-elongated filaments are often found in bundles, a situation which could allow dissociated formins to rapidly rebind to barbed ends. Also, recent studies have shown that regulatory proteins could directly bind to formins and modulate their activity (*e.g.,* Ena/VASP (Bilancia et al., 2014), CLIP170 (Henty-Ridilla et al., 2016), or Spire/FMN2 interactions (Montaville et al., 2014)). The stabilization of formin-filament interactions in a mechanical context by such proteins is an hypothesis that should be addressed in future experiments.

METHODS

Proteins and buffers

Skeletal muscle actin was purified from rabbit muscle acetone powder (Pel-freeze) following the protocol described in (Wioland et al., 2017), adapted from the original protocol (Spudich and Watt, 1971). Actin was fluorescently labeled on accessible surface lysine 328 of F-actin (Tóth et al., 2016), using Alexa 488-NHS (LifeTechnologies).
Recombinant human formin mDia1(SNAP-FH1-FH2-DAD-6xHis) was expressed in E. Coli Rosetta 2 (DE3) and purified following the protocol described in (Romero et al., 2004).
Recombinant human profilin I was expressed in E. Coli BL21 Star (DE3) and purified following the protocol described in details in (Wioland et al., 2017), based on the original protocol by (Gieselmann et al., 1995).
Spectrin-actin seeds were purified from human erythrocytes as described in (Wioland et al., 2017), based on the original protocol by (Casella et al., 1986).
Experiments were performed in F-buffer (5 mM Tris-HCl pH 7.8, 1 mM MgCl2, 0.2 mM EGTA, 0.2 mM ATP, 10 mM DTT and 1 mM DABCO) with various concentrations of KCl, as indicated in the main text and figures.

Microfluidics setup and experiments

Protein solutions were injected into a Poly-Dimethyl-Siloxane (PDMS, Sylgard) chamber, 20 µm or 40 µm in height, 800 µm in width and 1 cm in length. Chambers were mounted on glass coverslips previously cleaned for 20 minutes in ultrasonic baths of 1M KOH, ethanol and dH20. PDMS chambers and glass coverslips were UV-treated (UVO cleaner, Jelight) to allow them to bind tightly to each other. We used cross-shaped channels with 3 inlets. We controlled the pressure in the reservoir and measured the flow rate in each channel using an MFCS and Flow Units (Fluigent).
For experiments with anchored pointed ends (configurations shown in Figure 1A,B) the chamber was first filled with F-buffer without KCl. We then injected actin-spectrin seeds, 10 pM for 5 min, which adsorbed to the glass surface non-specifically. The surface was then passivated with 5% bovine serum albumin for at least 10 min.
The anchoring of formins to the coverslip surface (configurations shown in Figures 1C and 4A) was achieved in various ways, with similar results. Surfaces were first passivated and functionalized with biotin, either with PLL-PEG containing a fraction of PLL-PEG-biotin (SuSoS, Switzerland) or with a mixture of BSA and biotinylated BSA. The surfaces were then incubated for 5 minutes with neutravidin (20 µg/mL) and rinsed. The various formin constructs all contained a C-terminal 6xHis tag to anchor them via a biotinylated anti-His (penta-His, Qiagen). To anchor specifically the mDia1 (FH1-FH2-DAD) via its N-terminus, we used a biotinylated SNAP-tag construct.

Microscopy and image acquisition

The microfluidic setup was placed on a Nikon TiE inverted microscope, equipped with a 60x oil-immersion objective. We either used TIRF, HiLo or epifluorescence depending on the background fluorophore concentration in solution. Two different TiE microscope setups were used. The TIRF setup was controlled by Metamorph, illuminated in TIRF or epifluorescence by 100mW tunable lasers (iLAS2, Roper Scientific), and images were acquired by an Evolve EMCCD camera (Photometrics). The other TiE setup was controlled by micromanager (Edelstein et al., 2014), illuminated with a 200W Xcite lamp (Lumen dynamics) and images were acquired by an sCMOS Orca-Flash4.0 V2+ camera (Hamamatsu).
Images were analyzed using ImageJ software.

The experiments were performed at room temperature, in an air-conditioned environment. We nonetheless measured day-to-day variations of room temperature, between 19°C and 23°C, and found that these temperature changes correlated with variations in filament elongation rates and formin dissociation rates : higher temperatures favored faster elongation and faster dissociation. To minimize the impact of such variations, and obtain consistent data, experiments and their controls were systematically repeated on the same day.

Data analysis

To avoid any bias related to the selection of filaments during analysis, a rectangular region containing a few tens of filaments was randomly chosen in the microscope field of view, and all the filaments in this region were analyzed. Within this population, filaments were excluded from our analysis only in the following specific cases. We excluded filaments whose ends were difficult to locate because they overlapped with other filaments. We also excluded filaments that sometimes seemed to stick to the surface or, in the case of experiments with anchored formins, appeared to stall (see Supp. Movies).

Movies were analyzed with ImageJ. The Subtract Background plugin was sometimes used to enhance the contrast, with a rolling ball radius of 50 pixels.

Quantifying error bars on the formin dissociation rates, in the absence of force.

In order to quantify the statistical uncertainty in the estimation of the dissociation rate k_{off} resulting from the exponential fits of the survival fractions *S(t)* (shown for example in Figures 1E and 2A,B), we performed numerical simulations of the experiment (using Python). The program simulated a large number (*M*=10,000) of experiments, each consisting in *N* filaments randomly losing their formin with rate constant k_0. The survival fraction of each experiment was fitted by a single exponential, resulting in the generation of *M* estimated rates k_{est} . The distribution of these k_{est} , centered on k_0, allowed us to compute the width of the confidence intervals. We could thus verify that a 65% confidence interval corresponded to errors of approximately $k_0/N^{0.5}$.

Analysis of experiments with striped filaments

Our standard experiment (Figure 1A) relied on the ability to image filaments and on the acceleration of their elongation by formins in order to assess their presence at the barbed end. In order to determine the elongation velocity and the formin dissociation rate in conditions where actin could not be directly imaged (i.e. unlabeled actin) and/or when the presence of formin was not readily detected by a change in elongation velocity (i.e. in the absence of profilin), other configurations were used. A possible alternative was to anchor the formins to the coverslip surface and work with low forces (Figure 1C). In order to obtain results with unanchored formins and zero force, we have used a “striped filaments” protocol (illustrated in Figure 1B). It consisted in exposing filaments to alternating conditions : a duration Δt_1 with condition 1 (the condition of interest, with unknown elongation rate v_1 and formin dissociation rate k_1), and a duration Δt_2 with condition 2 (containing profilin and labeled actin, with predetermined elongation rate v_2 and formin dissociation rate k_2). The resulting, striped filament population was imaged at interval ($\Delta t_1+\Delta t_2$) and had a measurable elongation rate $v=(\Delta t_1 v_1+\Delta t_2 v_2)/(\Delta t_1+\Delta t_2)$ and formin dissociation rate $k=(\Delta t_1 k_1+\Delta t_2 k_2)/(\Delta t_1+\Delta t_2)$. Knowing v_2 and k_2, we could thus determine v_1 and k_1. The results we obtained were consistent with those from experiments with anchored formins, at very low force.

Analysis of experiments with pulling forces

We measured the fraction *S(t)* of filaments growing from surface-anchored formins that remained attached over time, while force was applied on the filaments by viscous drag. The observed filament detachment rate $k_{obs}(t) = (dS/dt) / S(t)$ increases over time, as the filaments get longer and the average force exerted on them thus increases. This force has been calibrated (Jégou et al., 2013) and we can compute the average force *f(t)* exerted on the population of filaments, homogeneous in length.

An important point is to verify whether the filament detachment events that we observe during our experiment do correspond to formin-filament dissociation events. We thus sought to estimate what percentage of the monitored formins were still present and functional at the end of an experiment. To do so, following the experiment, we exposed the surface to a solution of actin to test which formins could nucleate new filaments. We observed that ~ 74% of formins were still present and able to nucleate filaments during this test (Supp. Fig. S4), regardless of the force applied during the experiment (between 0 and 6 pN). This indicated that at least 74% of the formins monitored during the experiment were still anchored and functional when their filament was observed to detach from the surface.The measured filament detachment rate k_{obs} thus reflected the formin dissociation rate k_{off} within a reasonable error: $0.74\ k_{obs} < k_{off} < k_{obs}$ (corresponding to the vertical error bars shown in Supp. Fig. S3).

We could thus plot the formin dissociation rate k_{off} as a function of the applied force *f*. Each individual experiment generated a survival fraction *S(t)* (as in Figure 4B) from which we deduced a number of points $k_{off}(f)$, as shown in Supp Fig S3. The horizontal error bars indicate the standard deviations in f, based on the length dispersion of the filaments. Experiments carried out with different microfluidics flow rates explored different ranges of force, with some overlap between experiments. For clarity, data points were grouped in bins of similar force, and averaged. The resulting plots are shown in Figure 4, where the error bars indicate the standard deviations for *f* and for k_{off} within each bin.

ACKNOWLEDGEMENTS

The authors acknowledge funding from the Fondation pour la Recherche Médicale (grant to G.R.L and M.L.), the Human Frontier Science Program (grant RGY0066 to G.R.L.), the European Research Council (grant StG-679116 to A.J.) and the Fondation ARC pour la Recherche sur le Cancer (postdoctoral fellowship to H.W.).

AUTHOR CONTRIBUTIONS

MK, LC, ES, GRL and AJ performed experiments; MK, LC, ES, HW, ML, GRL and AJ analyzed data; LC, SJ and BG supplied reagents; GRL and AJ supervised the project; ML, GRL and AJ and wrote the paper with input from all authors.

COMPETING INTERESTS

The authors declare no competing interests.

References:

Baker, J.L., Courtemanche, N., Parton, D.L., McCullagh, M., Pollard, T.D., and Voth, G.A. (2015). Electrostatic interactions between the Bni1p Formin FH2 domain and actin influence actin filament nucleation. Structure *23*, 68–79.

Bilancia, C.G., Winkelman, J.D., Tsygankov, D., Nowotarski, S.H., Sees, J.A., Comber, K., Evans,

I., Lakhani, V., Wood, W., Elston, T.C., et al. (2014). Enabled negatively regulates diaphanous-driven actin dynamics in vitro and in vivo. Dev. Cell *28*, 394–408.

Blanchoin, L., Boujemaa-Paterski, R., Sykes, C., and Plastino, J. (2014). Actin Dynamics, Architecture, and Mechanics in Cell Motility. Physiol. Rev. *94*, 235–263.

Bombardier, J.P., Eskin, J.A., Jaiswal, R., Corrêa, I.R., Jr, Xu, M.-Q., Goode, B.L., and Gelles, J. (2015). Single-molecule visualization of a formin-capping protein /`decision complex/' at the actin filament barbed end. Nat. Commun. *6*.

Bovellan, M., Romeo, Y., Biro, M., Boden, A., Chugh, P., Yonis, A., Vaghela, M., Fritzsche, M., Moulding, D., Thorogate, R., et al. (2014). Cellular control of cortical actin nucleation. Curr. Biol. *24*, 1628–1635.

Casella, J.F., Maack, D.J., and Lin, S. (1986). Purification and initial characterization of a protein from skeletal muscle that caps the barbed ends of actin filaments. J. Biol. Chem. *261*, 10915–10921.

Chen, Q., Nag, S., and Pollard, T.D. (2012). Formins filter modified actin subunits during processive elongation. J. Struct. Biol. *177*, 32–39.

Chesarone, M., Gould, C.J., Moseley, J.B., and Goode, B.L. (2009). Displacement of formins from growing barbed ends by bud14 is critical for actin cable architecture and function. Dev. Cell *16*, 292–302.

Chesarone-Cataldo, M., Guérin, C., Yu, J.H., Wedlich-Soldner, R., Blanchoin, L., and Goode, B.L. (2011). The Myosin Passenger Protein Smy1 Controls Actin Cable Structure and Dynamics by Acting as a Formin Damper. Dev. Cell *21*, 217–230.

Choi, J.-A., Jung, Y.S., Kim, J.Y., Kim, H.M., and Lim, I.K. (2015). Inhibition of breast cancer invasion by TIS21(/BTG2/Pc3)-Akt1-Sp1-Nox4 pathway targeting actin nucleators, mDia genes. Oncogene.

Courtemanche, N., and Pollard, T.D. (2012). Determinants of Formin Homology 1 (FH1) domain function in actin filament elongation by formins. J. Biol. Chem. *287*, 7812–7820.

Courtemanche, N., Lee, J.Y., Pollard, T.D., and Greene, E.C. (2013). Tension modulates actin filament polymerization mediated by formin and profilin. Proc. Natl. Acad. Sci. U. S. A. *110*, 9752–9757.

Edelstein, A.D., Tsuchida, M.A., Amodaj, N., Pinkard, H., Vale, R.D., and Stuurman, N. (2014). Advanced methods of microscope control using μManager software. J Biol Methods *1*.

Gould, C.J., Maiti, S., Michelot, A., Graziano, B.R., Blanchoin, L., and Goode, B.L. (2011). The formin DAD domain plays dual roles in autoinhibition and actin nucleation. Curr. Biol. *21*, 384–390.

Henty-Ridilla, J.L., Rankova, A., Eskin, J.A., Kenny, K., and Goode, B.L. (2016). Accelerated actin filament polymerization from microtubule plus ends. Science *352*, 1004–1009.

Higashida, C., Miyoshi, T., Fujita, A., Oceguera-Yanez, F., Monypenny, J., Andou, Y., Narumiya, S., and Watanabe, N. (2004). Actin polymerization-driven molecular movement of mDia1 in living

cells. Science *303*, 2007–2010.

Isogai, T., and Innocenti, M. (2016). New nuclear and perinuclear functions of formins. Biochem. Soc. Trans. *44*, 1701–1708.

Jégou, A., Niedermayer, T., Orbán, J., Didry, D., Lipowsky, R., Carlier, M.-F., and Romet-Lemonne, G. (2011). Individual actin filaments in a microfluidic flow reveal the mechanism of ATP hydrolysis and give insight into the properties of profilin. PLoS Biol. *9*, e1001161.

Jégou, A., Carlier, M.-F., and Romet-Lemonne, G. (2013). Formin mDia1 senses and generates mechanical forces on actin filaments. Nat. Commun. *4*, 1883.

Kovar, D.R., and Pollard, T.D. (2004). Insertional assembly of actin filament barbed ends in association with formins produces piconewton forces. Proc. Natl. Acad. Sci. U. S. A. *101*, 14725–14730.

Kovar, D.R., Harris, E.S., Mahaffy, R., Higgs, H.N., and Pollard, T.D. (2006). Control of the assembly of ATP- and ADP-actin by formins and profilin. Cell *124*, 423–435.

Kubota, H., Miyazaki, M., Ogawa, T., Shimozawa, T., Kinosita, K., Jr, and Ishiwata, S. 'ichi (2017). Biphasic Effect of Profilin Impacts the Formin mDia1 Force-Sensing Mechanism in Actin Polymerization. Biophys. J. *113*, 461–471.

Kuhn, J.R., and Pollard, T.D. (2005). Real-time measurements of actin filament polymerization by total internal reflection fluorescence microscopy. Biophys. J. *88*, 1387–1402.

Mizuno, H., Higashida, C., Yuan, Y., Ishizaki, T., Narumiya, S., and Watanabe, N. (2011). Rotational movement of the formin mDia1 along the double helical strand of an actin filament. Science *331*, 80–83.

Montaville, P., Jégou, A., Pernier, J., Compper, C., Guichard, B., Mogessie, B., Schuh, M., Romet-Lemonne, G., and Carlier, M.-F. (2014). Spire and Formin 2 synergize and antagonize in regulating actin assembly in meiosis by a ping-pong mechanism. PLoS Biol. *12*, e1001795.

Niedermayer, T., Jegou, A., Chièze, L., Guichard, B., Helfer, E., Romet-Lemonne, G., Carlier, M.-F., and Lipowsky, R. (2012). Intermittent depolymerization of actin filaments is caused by photo-induced dimerization of actin protomers. Proceedings of the National Academy of Sciences *109*, 10769–10774.

Otomo, T., Tomchick, D.R., Otomo, C., Panchal, S.C., Machius, M., and Rosen, M.K. (2005). Structural basis of actin filament nucleation and processive capping by a formin homology 2 domain. Nature *433*, 488–494.

Paul, A., and Pollard, T.D. (2008). The role of the FH1 domain and profilin in formin-mediated actin-filament elongation and nucleation. Curr. Biol. *18*, 9–19.

Pernier, J., Shekhar, S., Jegou, A., Guichard, B., and Carlier, M.-F. (2016). Profilin Interaction with Actin Filament Barbed End Controls Dynamic Instability, Capping, Branching, and Motility. Dev. Cell *36*, 201–214.

Phng, L.-K., Gebala, V., Bentley, K., Philippides, A., Wacker, A., Mathivet, T., Sauteur, L., Stanchi, F., Belting, H.-G., Affolter, M., et al. (2015). Formin-mediated actin polymerization at endothelial

junctions is required for vessel lumen formation and stabilization. Dev. Cell *32*, 123–132.

Romero, S., Le Clainche, C., Didry, D., Egile, C., Pantaloni, D., and Carlier, M.-F. (2004). Formin is a processive motor that requires profilin to accelerate actin assembly and associated ATP hydrolysis. Cell *119*, 419–429.

Romet-Lemonne, G., and Jégou, A. (2013). Mechanotransduction down to individual actin filaments. Eur. J. Cell Biol. *92*, 333–338.

Roos, A., Weis, J., Korinthenberg, R., Fehrenbach, H., Häusler, M., Züchner, S., Mache, C., Hubmann, H., Auer-Grumbach, M., and Senderek, J. (2015). Inverted formin 2-related Charcot-Marie-Tooth disease: extension of the mutational spectrum and pathological findings in Schwann cells and axons. J. Peripher. Nerv. Syst. *20*, 52–59.

Shekhar, S., Kerleau, M., Kühn, S., Pernier, J., Romet-Lemonne, G., Jégou, A., and Carlier, M.-F. (2015). Formin and capping protein together embrace the actin filament in a ménage à trois. Nat. Commun. *6*, 8730.

Spudich, J.A., and Watt, S. (1971). The regulation of rabbit skeletal muscle contraction. I. Biochemical studies of the interaction of the tropomyosin-troponin complex with actin and the proteolytic fragments of myosin. J. Biol. Chem. *246*, 4866–4871.

Tóth, M.Á., Majoros, A.K., Vig, A.T., Migh, E., Nyitrai, M., Mihály, J., and Bugyi, B. (2016). Biochemical Activities of the Wiskott-Aldrich Syndrome Homology Region 2 Domains of Sarcomere Length Short (SALS) Protein. J. Biol. Chem. *291*, 667–680.

Vavylonis, D., Kovar, D.R., O'Shaughnessy, B., and Pollard, T.D. (2006). Model of formin-associated actin filament elongation. Mol. Cell *21*, 455–466.

Vizcarra, C.L., Bor, B., and Quinlan, M.E. (2014). The Role of Formin Tails in Actin Nucleation, Processive Elongation, and Filament Bundling. J. Biol. Chem.

Wales, P., Schuberth, C.E., Aufschnaiter, R., Fels, J., García-Aguilar, I., Janning, A., Dlugos, C.P., Schäfer-Herte, M., Klingner, C., Wälte, M., et al. (2016). Calcium-mediated actin reset (CaAR) mediates acute cell adaptations. Elife *5*.

Wioland, H., Guichard, B., Senju, Y., Myram, S., Lappalainen, P., Jégou, A., and Romet-Lemonne, G. (2017). ADF/Cofilin Accelerates Actin Dynamics by Severing Filaments and Promoting Their Depolymerization at Both Ends. Curr. Biol. *27*, 1956–1967.e7.

Yu, M., Yuan, X., Lu, C., Le, S., Kawamura, R., Efremov, A.K., Zhao, Z., Kozlov, M.M., Sheetz, M., Bershadsky, A., et al. (2017). mDia1 senses both force and torque during F-actin filament polymerization. Nat. Commun. *8*, 1650.

Zimmermann, D., Homa, K.E., Hocky, G.M., Pollard, L.W., De La Cruz, E.M., Voth, G.A., Trybus, K.M., and Kovar, D.R. (2017). Mechanoregulated inhibition of formin facilitates contractile actomyosin ring assembly. Nat. Commun. *8*, 703.

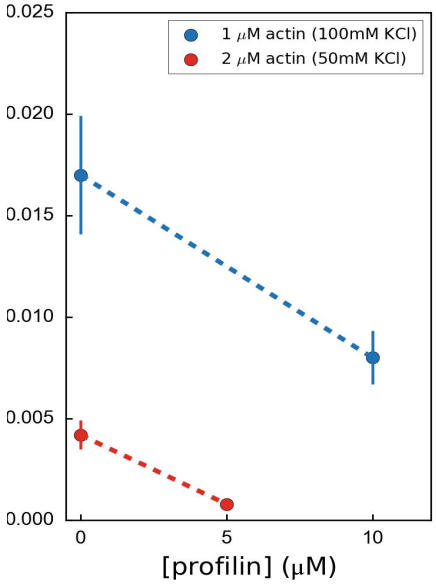

Supp Figure S1:
Variation of the formin mDia1(FH1-FH2-DAD) dissociation rate as a function of profilin concentration, for 2μM unlabeled actin at 50mM KCl (red) or for 1μM unlabeled actin at 100mM KCl (blue), showing that formin processivity is decreased by profilin with unlabeled actin, for both salt conditions.

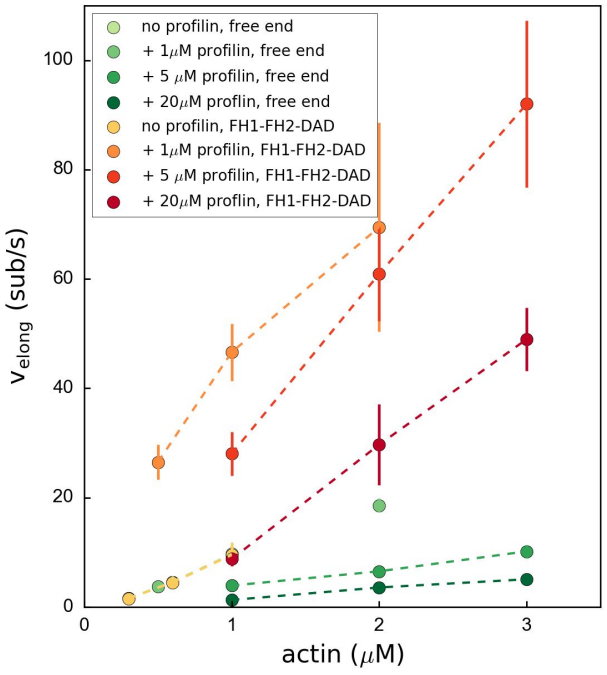

Supp Figure S2:
Variation of the formin-bound or free barbed end elongation rate v_{elong} as a function of actin concentration. Each data point corresponds to an independent experiment (N=30-40 filaments) which was conducted at 100mM KCl. Error bars indicate standard deviations.

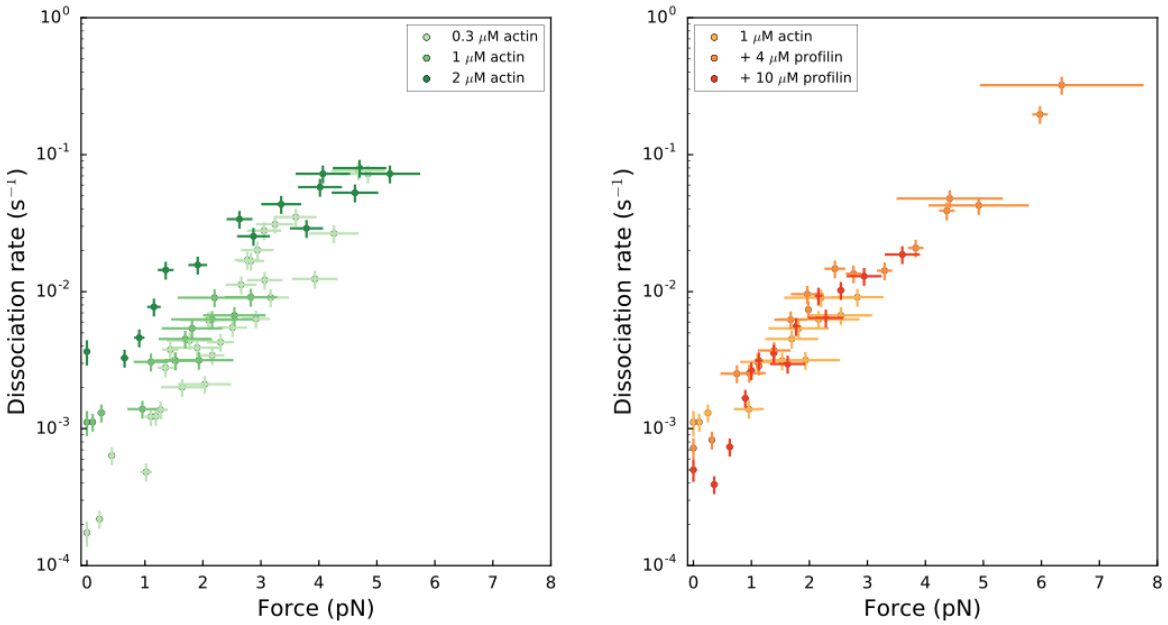

Supp Figure S3:
Formin dissociation rate as a function of applied force (log-linear plots): for different actin concentrations in the absence of profilin (left); for 1 μM actin with different profilin concentrations (right). Dissociation rates were obtained by local fits of the slope in survival fractions similar to the ones shown in Figure 4B (see Methods). Each data point is obtained from a single experiment. Error bars indicate the standard deviations for force and the +/- 0.13% uncertainty on the dissociation rate, accounting for formin detachments from the surface (see Methods). Grouping these data in bins of similar forces resulted in the plots shown in Figures 4C and 4D.

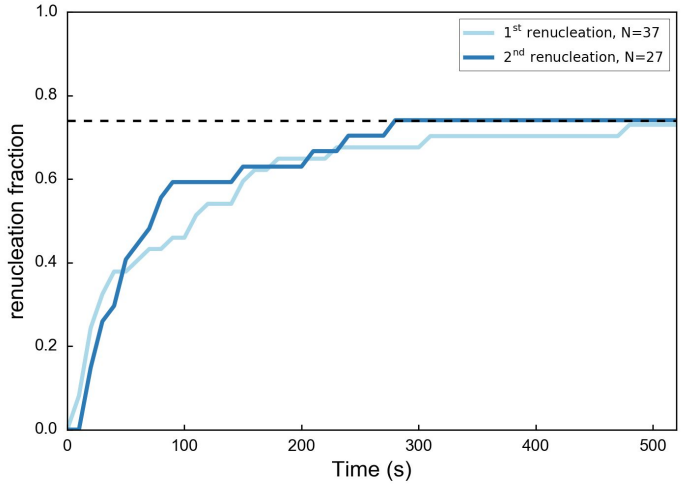

Supp Figure S4:
Nucleation of new filaments from surface-anchored formins. The anchored mDia1(FH1-FH2-DAD) formins that participated in a pulling force experiment with 1μM actin 4μM profilin in a moderate flow (i.e. reaching a pulling force ~ 1-4 pN before filaments detached) as depicted in Figure 4, were subjected to a renucleation assay to assess if they were still present on the coverslip surface and functional. The renucleation assay consisted in exposing them alternatively, at the same flow rate, to a solution of F-buffer at 25mM KCl, 2μM 15% Alexa488-labeled actin, 0.4μM profilin and to a solution of F-buffer at 100mM KCl, 1μM unlabeled actin,

4μM profilin, for 15 seconds each. The formins that were observed renucleating a filament ("1st renucleation", light blue), eventually let go of that filament and could be observed nucleating another filament ("2nd renucleation", dark blue). The dashed line indicates that 74% of the formins had nucleated a new filament after 500 seconds.

MOVIE CAPTIONS

Movie S1. Actin filaments elongating with 1μM 15% Alexa488-labeled actin and 5 μM profilin, at 100 mM KCl, are transiently exposed to a solution of 20 nM mDia1(FH1-FH2-DAD) for 20 seconds (during frames 27-30). Images were acquired in TIRF. Full field of view is 137x137μm. Interval between images is 5 seconds (movie is accelerated 75x). The solution flows from left to right. Corresponds to Figure 1A of the main text.

Movie S2. Actin filaments are exposed to a periodic alternation of a solution of unlabeled actin (0.3 μM actin, 50 mM KCl) for 100 seconds and a solution of 15% Alexa488-labeled actin (0.5 μM actin + 2 μM profilin, 50 mM KCl) for 20 seconds. The filaments are transiently exposed to a solution of 11 nM mDia1(FH1-FH2-DAD) for 5 seconds, after frame number 5. Images were acquired in epifluorescence while exposing to unlabeled actin. Full field of view is 137x137μm. Interval between images is 120 seconds (movie is accelerated 360x). The solution flows from left to right. Corresponds to Figure 1B of the main text.

Movie S3. Actin filaments were nucleated from surface-anchored formins mDia1(FH1-FH2-DAD) with 15% Alexa488-labeled actin, and elongate with 0.3 μM unlabeled actin, at 50 mM KCl. Full field of view is 221x221μm. Images were acquired in epifluorescence. Interval between images is 10 seconds (movie is accelerated 70x). A minimal flow is applied (10 mbar pressure difference). The solution flows from left to right. Corresponds to Figure 1C of the main text.

Modulation of formin processivity by profilin and mechanical tension

—

Supplemental mathematical modeling

Mikaël Kerleau, Luyan Cao, Emiko Suzuki, Hugo Wioland, Sandy Jouet, Bérengère Guichard, Martin Lenz, Guillaume Romet-Lemonne, Antoine Jégou

Here we describe a mathematical model predicting the elongation velocity v_{elong} and dissociation rate k_{off} of a barbed-end associated formin as a function of actin and profilin concentrations c_a and c_p, as well as the force f applied to the formin in the direction of filament elongation. We present the model in Sec. S1 and derive its general predictions in Sec. S2. We then specialized these results to the measurements performed in the main text in Sec. S3.

As our model includes a substantial number of chemical reactions and associated reaction rates, we focus less on obtaining precise fits to the experimental data—which are somewhat trivial and uninformative when a large number of adjustable parameters are involved—and instead demonstrate that the *qualitative* shape of the curves predicted by our model is always consistent with our experimental measurements. This demonstrates that the agreement between our model and the data is essential, and not and accident of a specific set of values for the fitting parameters.

S1 Model description

The model is a kinetic description of the barbed end-formin complex based on transitions between three basic states. Following Ref. [1], we assume that formin can be associated with the filament barbed end in either a "closed" or an "open" conformation, of which only the latter allows for further filament elongation. These two states, henceforth abbreviated as C and O are assumed to be in rapid equilibrium, implying that their probabilities P_C and P_O are constrained by the detailed balance condition

$$\frac{P_O}{P_C} = \frac{\exp(-\beta\epsilon_O + \beta f\delta)}{\exp(-\beta\epsilon_C)} = \exp(-\beta\epsilon + \beta f\delta), \tag{S1}$$

where $\beta = 1/k_BT$ is the inverse thermal energy, $\epsilon = \epsilon_O - \epsilon_C$ is the energy difference between states O and C and δ is the average distance over which the formin moves along the filament as it transitions from C to O. Only state O allows the recruitment of a new actin monomer to the barbed end, which happens irreversibly with a rate $k_a c_a$ proportional to the actin concentration in solution. This monomer addition takes the system to a short-lived transient state, denoted by T. As schematized in Fig. 1(a), this state decays with a rate $1/\tau$ into a new fast $C \rightleftharpoons O$ equilibrium with one more actin monomer, implying that the new C state is shifted with respect to the original one by a distance δ, and similarly for O.

While the formin is bound to the actin in all three states, thermal agitation and the force f may pull it to the right and off the filament, implying formin dissociation. This may happen in state O or T, but not in state C, reflecting the fact that a formin starting from state C must first go through O before it can leave the filament. Denoting by δ_O and δ_T the distance over which the formin must be pulled to be ripped off the filament when in state O or T respectively, we assimilate the dissociation process to a simple Kramers escape problem and write the associated dissociation rates

$$k_{\text{off}}^O(f) = k_{\text{off}}^O(0) \times e^{\beta f\delta_O}, \qquad k_{\text{off}}^T(f) = k_{\text{off}}^T(0) \times e^{\beta f\delta_T}. \tag{S2}$$

To account for the possibility of profilin-actin association, we introduce profilin-associated versions of each of the aforementioned states, which we denote as $C^\bullet$, $O^\bullet$ and $T^\bullet$. In these states, the last actin on the filament barbed end is bound to a profilin, which sterically prevents the addition of any new actin monomer to the

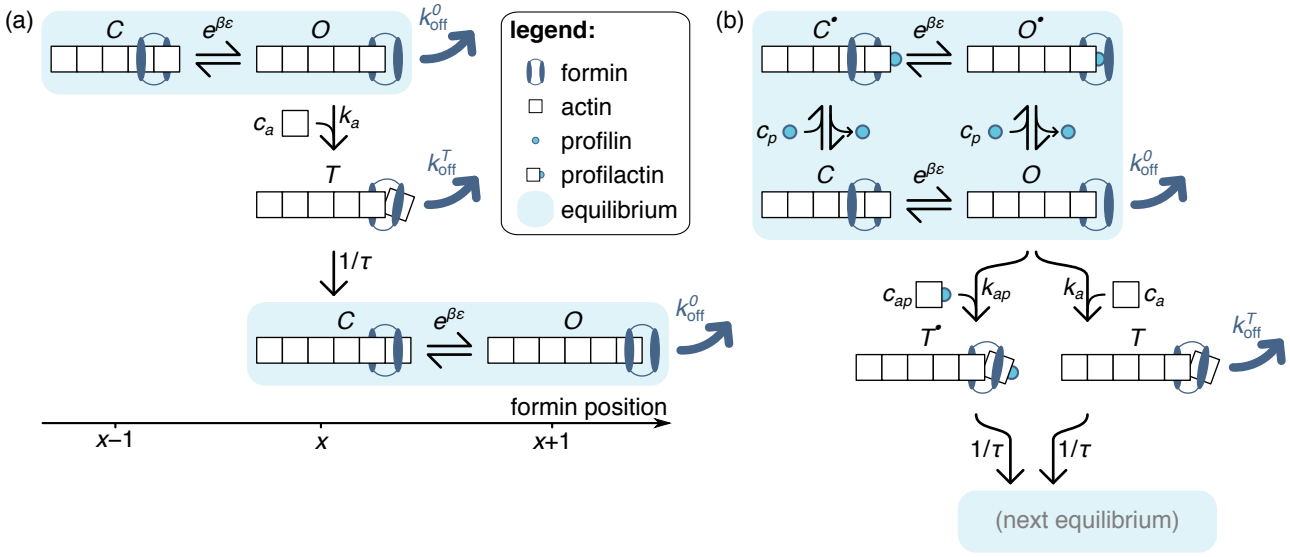

Figure 1: Model of formin function based on transitions between discrete states, as described in the text. Unlike those of the main text, the schematics presented here only picture one actin protofilament for simplicity, without any implications for the model itself. In both panels, formin dissociation from states O and T is indicated by thick dark blue arrows. The FH1 domains, which lead to the formation of a ring complex that hampers this dissociation in profilin-associated states, is not explicitely represented here. (a) Simplified, no-profilin model introducing the notion of rapid equilibrium between monomer additions, and transit through a short-lived state T upon monomer addition. (b) Model taking into account the association of profilin with the filament barbed end.

filament prior to its detachment. We denote by K_d the equilibrium dissociation constant of the following reaction

$$\text{(profilinated barbed end)} \rightleftharpoons \text{(barbed end)} + \text{(profilin)}. \tag{S3}$$

Combined with the assumption that states $C^\bullet$ and $O^\bullet$ are at a rapid equilibrium with states C and O, this implies

$$\frac{P_{C^\bullet}}{P_C} = \frac{P_{O^\bullet}}{P_O} = \frac{c_p}{K_d}, \tag{S4}$$

which we combine with Eq. (S1) and the normalization condition $P_{C^\bullet} + P_C + P_{O^\bullet} + P_O = 1$ to obtain

$$P_{C^\bullet} = \frac{e^{\beta\epsilon} c_p/K_d}{(1+c_p/K_d)(e^{\beta\epsilon}+e^{\beta f\delta})} \tag{S5a}$$

$$P_C = \frac{e^{\beta\epsilon}}{(1+c_p/K_d)(e^{\beta\epsilon}+e^{\beta f\delta})} \tag{S5b}$$

$$P_{O^\bullet} = \frac{e^{\beta f\delta} c_p/K_d}{(1+c_p/K_d)(e^{\beta\epsilon}+e^{\beta f\delta})} \tag{S5c}$$

$$P_O = \frac{e^{\beta f\delta}}{(1+c_p/K_d)(e^{\beta\epsilon}+e^{\beta f\delta})} \tag{S5d}$$

State $T^\bullet$, on the other hand, can only be reached by adding a profilactin to a filament barbed end in the O state, which occurs with rate $k_{ap}c_{ap}$, where c_{ap} denotes the profilactin concentration in solution. Similar to the behavior of state T, we assume that state $T^\bullet$ quickly transitions into a new $C^\bullet \rightleftharpoons C \rightleftharpoons O \rightleftharpoons O^\bullet$ equilibrium with a rate $1/\tau$.

As discussed in the main text, we assume that none of the profilinated states is amenable to formin dissociation, as the interactions between formin's FH1 domain and the filament-bound profilin helps stabilize its attachment to the filament.

S2 Elongation and dissociation rates

To compute the filament's average elongation rate, we compute the average time $1/v_{\text{elong}}$ required to add a monomer to it. When in the $C^\bullet \rightleftharpoons C \rightleftharpoons O \rightleftharpoons O^\bullet$ equilibrium, the system spends a fraction P_O of its time in the O state. During this time, it may transition into the T and $T^\bullet$ states with respective rates $k_a c_a$ and $k_{ap} c_{ap}$, implying an overall escape rate out of the equilibrium of $k_a c_a P_O + k_{ap} c_{ap} P_O$. Following our assumption that states $T^\bullet$ and T are short-lived, the time scale τ is negligible in front of the escape time and thus the elongation velocity (measured in number of monomers per unit time) reads

$$v_{\text{elong}} = k_a c_a P_O + k_{ap} c_{ap} P_O. \tag{S6}$$

Our model allows for two sources of formin dissociation. First, formin may leave the filament while in the O state. As formin spends a fraction P_O of its time in this state, the associated dissociation rate reads $k_{\text{off}}^O(f) P_O$. Second, formin may leave the filament while in the T state. While this state is very transient, it has been argued that it is also highly unstable [2] and thus that the associated dissociation rate may be significant. To estimate this dissociation rate, we first consider a system that has just transitioned into the T state. The system may escape this state through either one of two mechanisms, namely a transition into the $C^\bullet \rightleftharpoons C \rightleftharpoons O \rightleftharpoons O^\bullet$ equilibrium (with rate $1/\tau$), or dissociation [with rate $k_{\text{off}}^T(f)$]. Since both of these rates are constant over time, it is easy to show that the probability to escape the T state through dissociation is $k_{\text{off}}^T(f)\tau/[1 + k_{\text{off}}^T(f)\tau]$. Similarly, starting from the $C^\bullet \rightleftharpoons C \rightleftharpoons O \rightleftharpoons O^\bullet$ equilibrium the probability of entering the T state rather than the $T^\bullet$ state reads $k_a c_a/(k_a c_a + k_{ap} c_{ap})$, implying that the probability of losing the formin while transitioning from one equilibrium to the next reads

$$\frac{k_a c_a}{k_a c_a + k_{ap} c_{ap}} \times \frac{k_{\text{off}}^T(f)\tau}{1 + k_{\text{off}}^T(f)\tau} \tag{S7}$$

Finally, as there is on average one such transition per time interval of duration $1/v_{\text{elong}}$, the overall dissociation rate of the formin reads

$$\begin{aligned} k_{\text{off}} &= k_{\text{off}}^O(f) P_O + v_{\text{elong}} \frac{k_a c_a}{k_a c_a + k_{ap} c_{ap}} \frac{k_{\text{off}}^T(f)\tau}{1 + k_{\text{off}}^T(f)\tau} \\ &= \frac{e^{\beta f \delta}}{e^{\beta \epsilon} + e^{\beta f \delta}} \frac{1}{1 + c_p/K_d} \left[k_{\text{off}}^O(f) + k_a c_a \frac{k_{\text{off}}^T(f)\tau}{1 + k_{\text{off}}^T(f)\tau} \right], \end{aligned} \tag{S8}$$

where the first and second terms in the square brackets relate to the dissociation rate in the open and transient state, respectively.

S3 Specific predictions

Here we specialize the results of Eqs. (S6) and (S8) to experimentally relevant situations, showing robust agreement with the data of the main text. In the following we make the simplifying assumption that the equilibrium dissociation constant $\simeq 0.1\,\mu$M of the chemical equilibrium

$$\text{G-profilactin} \rightleftharpoons \text{G-actin} + \text{profilin} \tag{S9}$$

in solution is much smaller than the other relevant concentrations in the system (typically a few μM), or equivalently that an excess of profilin in solution with respect to actin implies that essentially all actin is associated with profilin, with a negligible concentration of residual non-associated actin. Denoting by [A] and [P] the nominal concentrations of actin and profilin initially introduced in the solution, this implies

$$c_a = \begin{cases} [\text{A}] - [\text{P}] & \text{if } [\text{A}] > [\text{P}] \\ 0 & \text{if } [\text{A}] < [\text{P}] \end{cases}, \quad c_p = \begin{cases} 0 & \text{if } [\text{A}] > [\text{P}] \\ [\text{P}] - [\text{A}] & \text{if } [\text{A}] < [\text{P}] \end{cases}, \quad \text{and} \quad c_{ap} = \begin{cases} [\text{P}] & \text{if } [\text{A}] > [\text{P}] \\ [\text{A}] & \text{if } [\text{A}] < [\text{P}] \end{cases}. \tag{S10}$$

Using this assumption, in the following sections we derive theoretical predictions corresponding to the three main experimental curves of the main text.

S3.1 Profilin concentration dependence of the elongation velocity

Plugging Eq. (S10) into Eq. (S6), we obtain

$$v_{\text{elong}} = \begin{cases} \frac{k_a [A] + (k_{ap} - k_a)[P]}{1 + e^{\beta \epsilon}} & \text{if } [\text{A}] > [\text{P}] \\ \frac{k_{ap} [\text{A}]}{1 + e^{\beta \epsilon}} \frac{1}{1 + ([\text{P}] - [\text{A}])/K_d} & \text{if } [\text{A}] < [\text{P}] \end{cases}. \tag{S11}$$

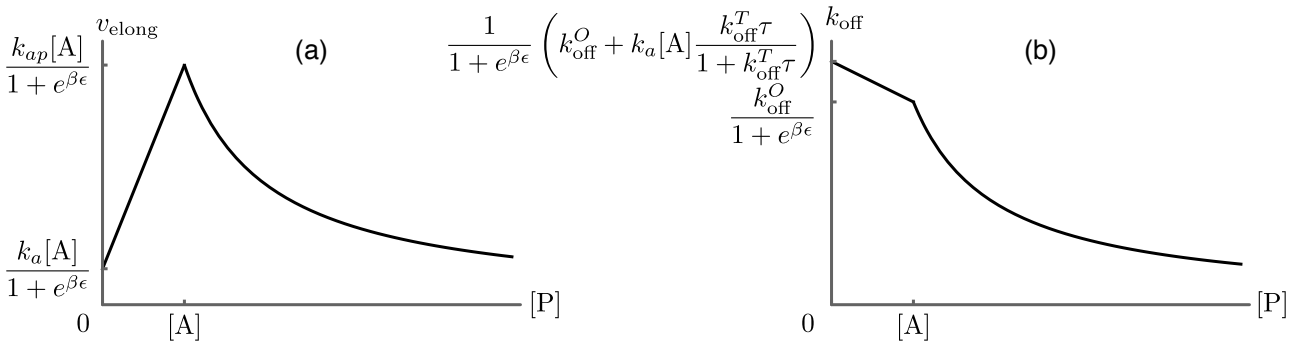

Figure 2: Predictions for the elongation velocity v_{elong} (a) and the formin dissociation rate k_{off} (b) as functions of the profilin concentration within the approximation of strong actin-profilin binding of Eq. (S10). While the exact position of the curves is dependent on the choice of parameters as indicated on the figure, their qualitative shapes are a robust prediction of the model, and agree well with the experimental data presented in Figure 3B of main text.

We represent this function in Fig. 2(a). Qualitatively, at low profilin the monomer addition rate is modest, with its pace set by the actin addition rate through the T pathway. As the profilin concentration is increased, the availability of profilactin subunits increases, leading to elongation with the faster rate k_{ap} through the $T^{\bullet}$ pathway. As the profilin concentration [P] exceeds the actin concentration [A], excess profilin accumulates in the solution, shifting the rapid equilibrium of Fig. 1 towards the $C^{\bullet}$ and $O^{\bullet}$ states, thus depleting the addition-competent O state and slowing down elongation.

S3.2 profilin concentration dependence of the dissociation rate

Plugging Eq. (S10) into Eq. (S8), we obtain

$$k_{\text{off}} = \begin{cases} \frac{1}{1+e^{\beta\epsilon}}\left[k_{\text{off}}^{O}+k_a([\text{A}]-[\text{P}])\frac{k_{\text{off}}^{T}\tau}{1+k_{\text{off}}^{T}\tau}\right] & \text{if } [\text{A}]>[\text{P}] \\ \frac{k_{off}^{O}}{1+e^{\beta\epsilon}}\frac{1}{1+([\text{P}]-[\text{A}])/K_d} & \text{if } [\text{A}]<[\text{P}] \end{cases}, \tag{S12}$$

which we plot in Fig. 2(b). Qualitatively, the formin dissociation rate is maximal at low profilin concentration, where all monomer additions occur through the dangerous T pathway. As [P] increases, an increasing number of T transitions are replaced by the safe $T^{\bullet}$ transitions, until at [P] = [A] the T transitions are entirely abrogated. At this and higher concentration, the only remaining cause of formin dissociation is through the O state, and as the profilin concentration is increased above [A], the occupancy of the O state decreases as described in Sec. S3.1, leading to a further decrease of the dissociation rate.

S3.3 Force dependence of the dissociation rate

To describe the force dependence of the formin dissociation rate, we introduce the force-dependent dissociation laws of Eq. (S2) into the dissociation rate of Eq. (S8) at [P] = 0. Based on our experimental observations, we restrict our discussion to situations where the formin stays bound to the barbed end for a number of monomer addition steps that is much larger than one, and thus to the regime $k_{\text{off}}^{T}(f)\tau \ll 1$, yielding

$$k_{\text{off}} = \frac{e^{\beta f\delta}}{e^{\beta\epsilon}+e^{\beta f\delta}}\left[k_{\text{off}}^{O}(0)e^{\beta f\delta_O}+k_a[\text{A}]k_{\text{off}}^{T}(0)e^{\beta f\delta_T}\tau\right] \tag{S13}$$

The two terms in the parenthesis of Eq. (S8) respectively correspond to dissociation from the O and from the T state. While both rates can contribute at small forces, for large forces the dominant contributor to the dissociation rate will be the process with the largest length scale δ_X (with $X = O$ or T), *i.e.*, dissociation through O if $\delta_O > \delta_T$, or dissociation through T if $\delta_T > \delta_O$. In the former case, the large-force asymptotic dissociation rate $k_{\text{off}} \sim k_{\text{off}}^{O}(0)e^{\beta f\delta_O}$ will be independent on the actin concentration, while in the latter $k_{\text{off}} \sim k_a[\text{A}]k_{\text{off}}^{T}(0)e^{\beta f\delta_T}\tau$ is proportional to it. As discussed in the main text, the dissociation *vs.* force curves for different actin concentrations converge at large force, indicating that the former hypothesis is correct, *i.e.*, that the force dependence of the dissociation rate in the O state is significantly larger than that in the T state. The corresponding theoretical curves are shown in Figure 5 of the main text.

References

[1] Takanori Otomo, Diana R Tomchick, Chinatsu Otomo, Sanjay C Panchal, Mischa Machius, and Michael K Rosen. Structural basis of actin filament nucleation and processive capping by a formin homology 2 domain. *Nature*, 433(7025):488–94, Feb 2005.

[2] Aditya Paul and Thomas Pollard. The role of the FH1 domain and profilin in formin-mediated actin-filament elongation and nucleation. *Curr. Biol.*, 18(1):9–19, January 2008.